Asian Journal of Pharmaceutical Sciences 19 (2024) 100940

Available online at www.sciencedirect.com

ScienceDirect

journal homepage: www.elsevier.com/locate/AJPS

Review Article

Vat-based photopolymerization 3D printing: From materials to topical and transdermal applications

Angélica Graça[1], *Sara Bom*[1], *Ana M. Martins, Helena M. Ribeiro, Joana Marto*[*]

Research Institute for Medicine (iMed.ULisboa), Faculty of Pharmacy, Universidade de Lisboa, Lisbon, Portugal

ARTICLE INFO

Article history:
Received 12 November 2023
Revised 30 January 2024
Accepted 18 March 2024
Available online 3 July 2024

Keywords:
Vat-based photopolymerization 3D printing
Topical delivery
Transdermal delivery
Resins
Photoinitiators

ABSTRACT

Three-dimensional (3D) printing is an innovative manufacturing method with the potential to revolutionize topical and transdermal dosage forms. Nowadays, it is established that Vat-based photopolymerization (VP) 3D printing technologies offer superior printing efficiency and versatility compared to other 3D printing technologies available on the market. However, there are some limitations that impair their full application in pharmaceutical contexts, such as the lack of a range of biocompatible materials for topical and transdermal applications. This review article explores all types of VP-based 3D printing and discusses the relevance of implementing this kind of technology. We start with a detailed description of the printing process, focusing on the commercial materials available and lab-made resins proposed by different authors. We also review recent studies in this field, which mainly focus on the fabrication of transdermal devices based on microneedle arrays. In the future, it is expected that the manufacturers of 3D printers invest in modifications to the printing apparatus to allow the simultaneous printing of different resins and/or compound types, which will open frontiers to the personalization of treatment approaches.

1. Introduction

Additive manufacturing (AM), commonly referred to as three-dimensional (3D) printing (3DP), is a revolutionary manufacturing process that constructs objects layer by layer. It was initially conceptualized in the mid-1980s by the American entrepreneur Charles W. Hull and has since experienced tremendous growth. Nowadays, 3DP offers a diverse array of techniques, each characterized by variations in materials, surface quality, durability, production speed, application processes, curing principles, and production costs [1–3].

The American Society for Testing and Materials (ISO/ASTM 52900:2015) plays a pivotal role in defining the terminology associated with AM. They have categorized 3D printing (3DP) into seven distinct types based on the underlying operational principles. These categories include powder-based printing (binder jet printing), extrusion-based printing (fused deposition modeling (FDM) and hydrogel-forming

* Corresponding author.
E-mail address: jmmarto@ff.ulisboa.pt (J. Marto).
[1] These authors contributed equally to this work.
Peer review under responsibility of Shenyang Pharmaceutical University.

https://doi.org/10.1016/j.ajps.2024.100940

extrusion (HFE)), stereolithographic printing (SLA), selective laser sintering printing (SLS), inkjet printing (IJ), and digital light processing (DLP) [2,4]. However, there are different classifications of 3DP. Nonetheless, alternative classification systems exist. For instance, Kafle et al. [4] have proposed a framework that groups 3D into three primary categories: solid-based, powder-based, and liquid-based, each comprising various subcategories, resulting in a total of eleven distinct categories. Solid-based 3DP encompasses laminar objective manufacturing, FDM, wire and arc AM, and electron beam freeform fabrication. Powder-based AM can be further divided into techniques like SLS, electron beam melting, selective laser melting, and laser metal deposition. Liquid-based methods encompass material jetting and Vat-based photopolymerization (VP) printing, including techniques such as SLA and DLP.

1.1. *VP-based 3D printing technology types: same principle, different results*

In 1986, SLA printing secured the first patent for a technology with commercial potential, marking a significant milestone in the world of AM. Its first creation was an eye-wash cup. However, the seeds of this technology were sown even earlier, in 1980, when Hideo Kodama, et al. working at the Nagoya Municipal Industrial Research Institute, sought a patent for a curing method utilizing ultraviolet (UV) light on photopolymer materials. Regrettably, this pioneering patent went unrealized due to a lack of funding for further research. Nevertheless, Kodama, et al. remains credited as the inventor of VP technology, making it the oldest form of AM [5]. VP-based technologies, in essence, rely on a light source to solidify liquid resin into a durable plastic form. However, within the realm of VP, there exist different subcategories, distinguished by the configuration of core components, such as the light source and the build platform (classified via elevation as bottom-up and top-down), and the resin tank [5,6]. Some of these distinct VP subcategories find applications in fields like topical and transdermal applications.

There are two primary categories of VP printing technologies, which can be classified according to curing method and way of elevation: SLA (laser-based/ top-down) and DLP (digital projection/ bottom-up) [4,5]. In SLA 3DP, a laser-based curing process is employed, utilizing a mirrored system. Here, a computer-controlled laser beam shapes structures, layer by layer, in a vector-by-vector and bottom-up fashion. The build platform is submerged in a vat of resin, and the laser traces the designated areas, curing the material according to the SLT template file. Once one layer is completed, the platform ascends in the z-direction, matching the height of each subsequent layer. The precision of SLA production is intricately tied to the diameter of the laser beam at the curing point [6,7]. Key factors influencing accurate and efficient SLA printing include scanning speed, laser power, exposure time, the choice of resin, the quantity of polymer, and the type and volume of photoinitiator (PI) used [5]. In contrast, DLP technology harnesses a digital light projector positioned beneath a transparent surface at the base of the resin vat. In this method, the entire layer is polymerized simultaneously when exposed to light. Consequently, the DLP process offers greater speed, and its precision hinges on the resolution of the projector [7,8]. This technology enables efficient and high-precision fabrication, with resolution capabilities spanning from 1 to 100 μm [9].

While SLA and DLP stand as the most used and recognized VP printing technologies, recent advancements have introduced alternatives with enhanced resolution and printing speed. One such innovation, inspired by DLP, is continuous digital light processing (CDLP) or continuous liquid interface production (CLIP), which employs an oxygen-based method of curing. This cutting-edge method incorporates a digital projection system akin to DLP but distinguishes itself by using a light-emitting diode (LED) and an oxygen-permeable window in lieu of the traditional glass window. What sets CDLP apart is its remarkable resolution, surpassing other VP technologies. This achievement is attributed to the oxygen-permeable window, which maintains a minuscule gap, as fine as a human hair, between the interface of the printed object and the window itself. This distance permits the unimpeded flow of liquid resin and significantly reduces the risk of printing failures. Furthermore, CDLP/CLIP is engineered for continuous movement of the build platform, achieving a remarkable print speed of approximately 100 mm per h. This makes it the fastest VP technology available to date, and it exhibits versatility in working with various materials to craft a wide range of objects with exceptional resolution [5,7].

In addition to CDLP/CLIP, another recent subcategory of VP technology is two-photon photopolymerization (TPP). This method facilitates the creation of intricate 3D structures in a single fabrication process, leveraging the inherent nonlinearity of multiphoton absorption. TPP employs a laser emission technique capable of producing 3D microstructures with resolutions that surpass the diffraction limit. This exceptional level of precision is achievable through the polymerization of a photosensitive polymeric resin, employing the two-photon absorption process. What sets TPP apart from other VP printers is its unique curing process. In TPP, the solid product is formed directly within the resin vat, eliminating the need for a layer-by-layer material deposition approach. Once the curing process is complete, any uncurable liquid resin is efficiently removed using an appropriate solvent, leaving behind the crafted 3D structure [7,10].

Microstereolithography (μSLA) is yet another noteworthy advancement in VP technology, designed to enhance the capabilities of DLP. Its primary goal is to increase resolution while retaining the capacity to produce larger or multiple components. This is achieved by incorporating a high-precision lens between the projector and the resin vat, enabling the build platform to move in the XY plane. This innovative approach allows for multiple imaging passes while upholding exceptional resolution using a top-down methodology. Remarkably, the μSLA system can attain an XY resolution of approximately 2 μm, with minimum feature sizes as small as 10 μm and dimensional tolerances as high as 10 μm [11].

For a concise overview of the VP technologies discussed above, Table 1 summarizes their key characteristics, including Z-axis resolution, accuracy, and printing speed.

Table 1 – Z-axis resolution, accuracy, and speed of different VP technologies.

Technology	Z-axis Resolution (μm)	Accuracy (μm)	Speed	Ref
SLA	10 – 200	0.5 - 50	20 – 36 mm/h	[6,7,12]
DLP	1 – 100	1 - 100	700 mm/h	[9,13]
CDLP/CLIP	50 – 100	0.5 - 50	1 – 5 μm/min	[5,7,12]
TPP	0.08 – 0.15	0.5 - 50	100 μm/min	[7,10,12]
μSLA	0.6 – 200	10 - 62	60 mm/h	[11,12]

Although the technologies described above are currently the most widely used for topical and transdermal applications, it is worth highlighting emerging technologies such as: (i) volumetric additive manufacturing (VAM), including computed axial lithography (CAL), which is inspired by the image reconstruction procedures of computed tomography (CT) [14] and dual-color photopolymerization (DCP), which follows xolographic principles [15]; and (ii) linear scan-based vat photopolymerization (LSVP) technology [16]. The VAM technologies have been proposed as gold standard solutions for evolving from nanoscopic to macroscopic length scales objects [15].

The subsequent sections provide a comprehensive look at the general composition of resins and offer an insight into the intricate polymerization chain reactions at play. Subsequently, we will delve into the advantages and constraints of these technologies, with a specific focus on their applicability to topical and transdermal applications.

1.2. *Resins and their general composition*

Two main types of resins are used for 3D printing: acrylate resins and epoxy resins. This review will only focus on acrylate resins and their polymerization process since topical applications mainly use this type of resin. This is because epoxy resins are known to cause allergic reactions, thus are unsuitable for topical applications. Acrylate resins utilized in VP 3DP consist of diminutive molecules known as monomers, serving as fundamental building blocks. These monomers possess structural characteristics that enable them to interconnect and assemble into chains through specific chemical reactions. It is important to emphasize that different monomers give different properties to the forming polymer. The polymerization process comprises three distinct phases: initiation, propagation, and termination [3,17].

In the initiation phase, monomers start connecting, forming oligomers. Subsequently, these chains extend, leading to the formation of polymers, each containing hundreds or even thousands of monomer subunits. Resins used in 3DP predominantly consist of multi-functional monomers based on methacrylate or acrylate esters. These monomers or oligomers exhibit not only swift reaction rates but also enduring stability and robust mechanical properties [3]. Furthermore, it is common practice to blend two or more types of monomers within resins. When this mixture undergoes polymerization, it generates co-polymers, resulting from chains composed of distinct monomer varieties. The distinctive properties of these co-polymers are contingent on the specific monomers present within the mixture (Fig. 1A).

Resins feature another vital component – crosslinkers. These molecules possess a structure with two or more connection points, areas that facilitate simultaneous bonding with two polymer chains (Fig. 1B). Crosslinkers can establish covalent or ionic bonds, serving as bridges linking one polymer chain to another [4]. Additionally, certain resins incorporate plasticizers into their formulation (Fig. 1B). These additives, often non-reactive diluents or liquid co-monomers, play a pivotal role in adjusting the viscosity of printable resins. While these molecules do not participate directly in the polymerization reaction, they occupy spaces between the chains within the final solid matrix, thus influencing the resin's viscosity. Suitable viscosities may range from 0.25 Pa·s for low molecular weight samples to 10 Pa·s for higher molecular weight samples, with most resins maintaining a viscosity of around 1 Pa·s. When viscosity requires modification for optimal performance, the introduction of plasticizers is an effective strategy, enhancing flexibility and averting excessive brittleness [18]. Pigments are another essential component in resins. These molecules, while not directly participating in the polymerization reaction, serve the purpose of providing color to the final printed product. The most employed colors in resins encompass shades of grey, white, black, transparent, turquoise, and blue [7].

Lastly, within the composition of resins, a critical element to mention is the PI, a catalyst responsible for initiating the polymerization reaction. PIs operate by absorbing UV radiation emitted by the printer, subsequently harnessing this energy to commence the polymerization process (Fig. 2A). Under the influence of UV light with a specific wavelength, ranging from 385 to 405 nm, depending on the PI used, PIs undergo a transformation, forming highly reactive species known as free radicals, characterized by unpaired electrons. These free radicals then play a catalytic role by engaging in chain reactions with monomers and/or oligomers [7]. PIs are indispensable in VP technology, primarily because a significant proportion of commonly used monomers do not possess the innate capability to generate free radicals upon exposure to UV light. The generation of free radicals can be achieved through α-cleavage, involving the rupture of the carbon-carbon bond adjacent to the carbon carrying the specified PI function, or via hydrogen abstraction, which may occur either intramolecularly or with the assistance of a co-initiator [17,19,20].

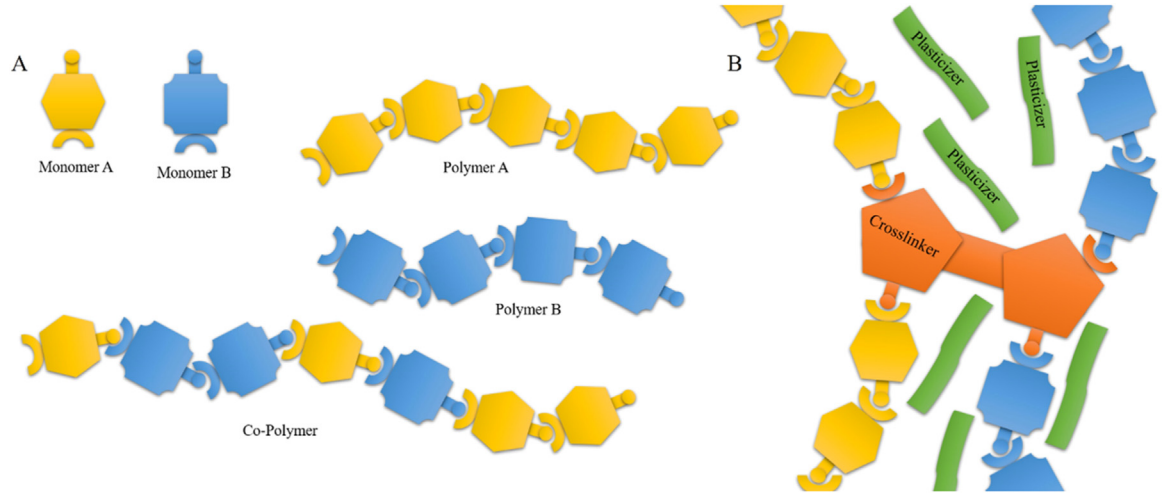

Fig. 1 – Schematic representation of components presented in a resin mixture: (A) monomers, polymers, and co-polymers, (B) crosslinkers and plasticizers.

1.3. *Polymerization chain reaction: the "skeleton" of 3D printed designs*

With all the components previously discussed, the polymerization chain reaction can be set into motion, as depicted in Fig. 2. When the PI absorbs UV light, it forms radicals, and these radicals readily interact with molecules that possess an even number of electrons, such as monomers or crosslinkers. This interaction gives rise to a new radical, creating another highly reactive molecule with an odd number of electrons. The unpaired electrons in this newly formed radical seek to pair up again to reach a lower energy state and readily engage with other atoms or molecules present within the resins, igniting a radical chain polymerization reaction [4,6,8].

Chain growth polymerization propagates until the point where a radical encounters another radical, culminating in the creation of a stable molecule with an even number of electrons. This interaction brings the reaction to an end. The result is the establishment of a complex crosslinked network, a process termed photocrosslinking (Fig. 2E) [4,6].

1.4. *Polymerization chain reaction and VP-based 3D printers: how does it work?*

In VP 3DP, the manufacturing process revolves around the principle of photopolymerization, wherein UV light is absorbed to solidify the photocurable liquid resin [4]. The intricate designs are crafted through a layer-by-layer methodology, where UV light meticulously irradiates the surface of the photosensitive resin, adhering to a precise pattern outlined in a computer-aided design (CAD) file [6,7]. In this process, the resin is contained within a vat, and a computer precisely coordinates the projection of a UV light pattern onto the transparent surface at the vat's base, where it interacts with the photosensitive resin. The region of the resin exposed to the light beam undergoes solidification as a result of the polymerization of monomers that occurs during the polymerization chain reaction. This transformation is irreversible, and once the first layer is polymerized, it firmly adheres to the printer-built platform, serving as a foundation for the subsequent structures as they are built. The platform is then incrementally moved to a predefined step height, with each new layer polymerizing beneath the preceding one (Fig. 3). The height of each layer and the printing speed are subject to variation depending on the specific type of VP technology employed (Table 1). This sequence of shifting the printer's platform and curing each layer individually is iteratively executed until the 3D structure specified in an STL file is fully realized [4,7,8].

The thickness of each layer in the printing process is contingent upon several factors, including the layer height, the energy applied, and the duration of exposure to the light source. The UV light used typically falls within a wavelength range of 300 nm to more than 400 nm. The overall quality of VP-printed items is significantly affected by key factors such as layer thickness, cure depth, and the efficacy of the post-curing process [4,7,8].

Balancing the curing depth (Cd) is critical in VP to strike a harmonious equilibrium. It should be sufficiently high to prevent prolonged manufacturing durations while avoiding over-polymerization, which can lead to diminished resolution. The Cd depends on the energy of the UV light applied to the resin and the duration of exposure. Its calculation relies on the Beer–Lambert law, as expressed in the following equation:

$$Cd = Dp \log E/Ec$$

where *Dp* is the penetration depth (m), *E* is the light exposure (J/m^2), and *Ec* is the critical light exposure (J/m^2) [21].

In the context of these technologies, post-curing is often an essential final step in the production of 3D designs. Once a design is fully printed, it remains affixed to the built platform. However, due to the possibility that certain parts may not have undergone complete polymerization during the initial printing phase, the design's full mechanical properties are yet

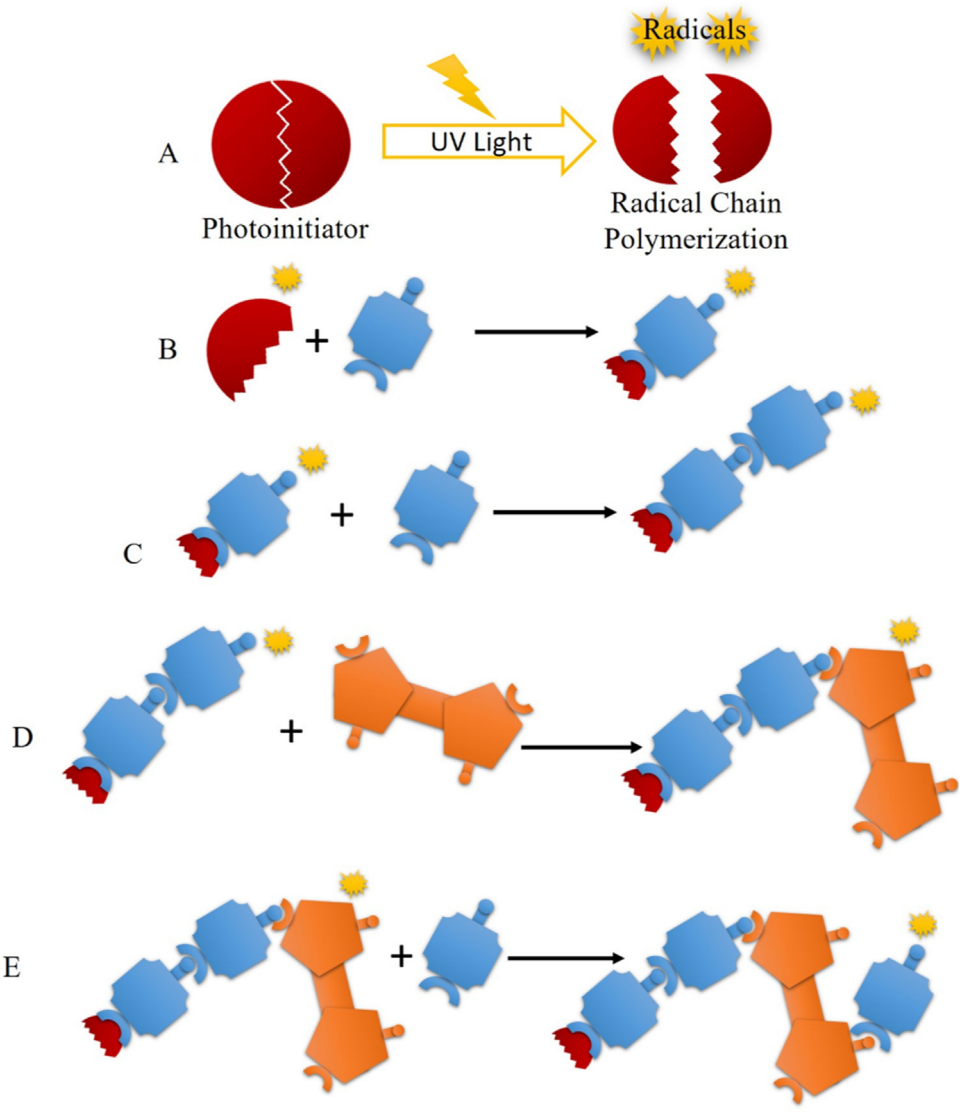

Fig. 2 – Schematic representation of the polymerization chain reaction steps. (A) PI and the formation of radical species from UV light absorption; (B) reaction between the PI and a monomer; (C) between a monomer and another monomer forming an oligomer; (D) between the oligomer and a crosslinker; (E) between the crosslinker and a monomer; finally, photocrosslinking process forming a stable polymer chain.

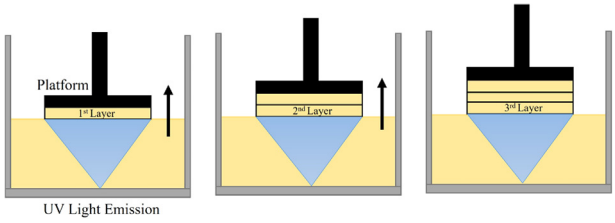

Fig. 3 – Overview of VP-based 3D printing principle showing the platform movement during the manufacturing printing process.

to be realized. The post-curing step is employed to optimize the mechanical properties of the printed product through a precise combination of temperature and light emission. The specific duration and energy requirements for ensuring a thorough post-curing process are contingent upon the intricacies of the printed design, and some products may need more post-curing time than others [21]. During the post-processing step, which includes cleaning procedures, isopropyl alcohol is commonly used to dissolve any remaining liquid resin that has not undergone polymerization. This practical approach is employed to effectively wash and clean away any residual resin, contributing to the refinement and finalization of the 3D printed product.

2. Commercially available resins

Commercially available resins are characterized by several common mechanical properties, including smooth surface

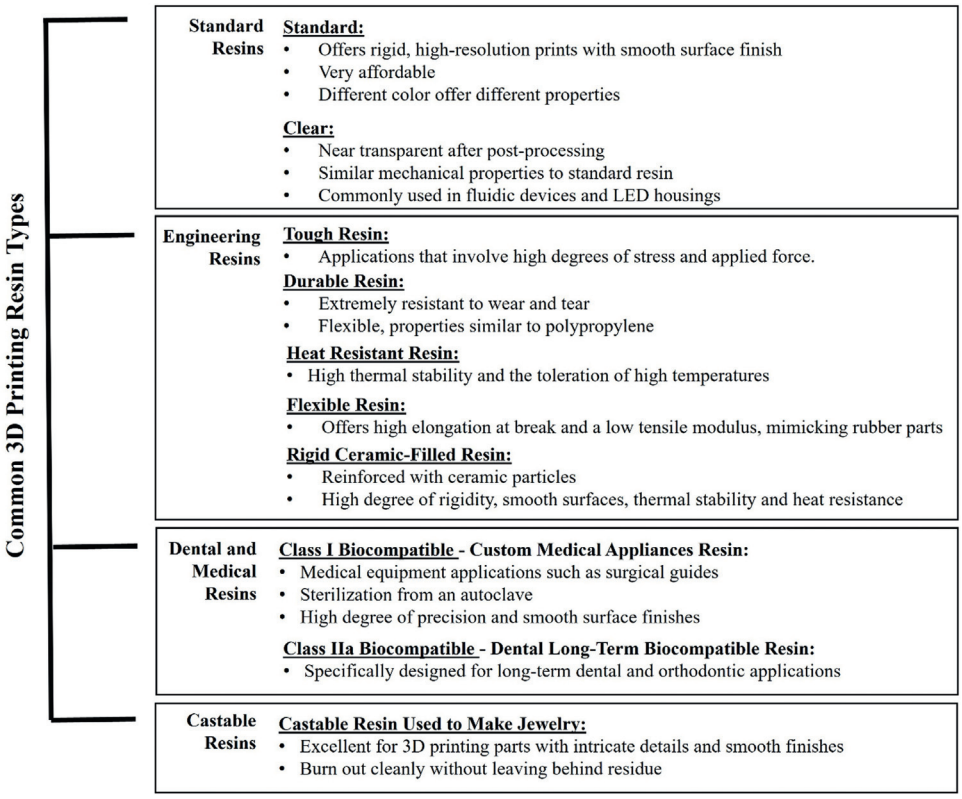

Fig. 4 – Common 3D printing resins and their characteristics and applications.

finishes, structural rigidity, and the capability to produce products with finely detailed features. The 3DP company 3DS (Dassault Systèmes SE, France), offering software solutions that enable the creation of groundbreaking products and services through the virtual 3DExperience platform, categorizes resins into four primary groups: Standard resins, Engineering resins, Dental and Medical resins, and Castable resins (Fig. 4) [22].

At present, numerous companies are actively engaged in the supply and manufacture of 3D printers employing diverse technologies. Among them, the American company Formlabs has emerged as a prominent leader, being the largest provider of professional SLA and SLS 3D printers on a global scale. Formlabs has garnered widespread recognition, ranking as one of the most frequently cited companies in published papers pertaining to 3DP [23]. We researched which VP technology companies were most cited in the literature pertaining to topical applications, and compiled and presented their available resins in Table 2. This compilation considers the classification scheme illustrated in Fig. 4 [24–27]. For instance, Dental LT Clear (Formlabs), noted for its suitability in transdermal applications, shows high optical transparency and flexural strength, facilitating a print resolution of 100 µm. This resin formulation comprises a mixture of methacrylic acid esters, where the PI composition comprises roughly 70% methacrylic oligomer, 20% glycol methacrylate, 5% pentamethyl-piperidyl sebacate, and 5% phosphine oxide [28].

3. VP-based 3D printing in topical and transdermal contexts

3.1. *Advantages and limitations*

The primary pharmaceutical application of VP 3DP technologies lies in the production of topical patches and transdermal devices, often incorporating microneedle (MN) arrays. In this domain, VP technologies offer superior printing efficiency and versatility when compared to other 3DP methods available in the market, such as FDM and HFE. These advantages encompass shorter print durations, stronger interlayer bonding, high surface finish, precision, and resolution, coupled with the freedom to create intricate designs featuring micron-sized structures, with some reaching down to 0.2 µm and complex internal geometries [5,29,30]. Much of these capabilities are attributed to the use of light or laser-based crosslinking methods, which provide superior spatial control and flexibility in the manufacturing process.

However, there are differences in terms of printability and resolution within VP technologies. A study conducted by Mathew et al. [31] explored the printability of three resin-based 3DP techniques, namely DLP, SLA and liquid crystal display (LCD). Specific resins were employed for each technique, with PlasGRAY resin (Asiga, Alexandria, Australia) used for DLP, Dental SG resin for SLA and UV White/Ivory

Table 2 – Commercially available VP technology resins and supplier companies.

Company	Standard Resins	Engineering Resins	Dental and Medical Resins	Castable Resins
Formlabs (SLA)	Black; White;Clear;Color Base; Draft; Grey Grey Pro	Ceramic; Durable; ESD; Elastic 50A; Flexible 80A; Rigid 10 K; Rigid 4000; Tough 2000; Tough 1500; High Temp; PU Rigid 1000; PU Rigid 650; Rebound	BioMed Amber; BioMed Black; BioMed Clear; BioMed White; Custom Tray; Dental LT Clear; Dental LT Clear (V2); Dental SG; Digital Dentures; Model; IBT; Surgical Guide; Temporary CB; Permanent Crown; Denture Base + Teeth; Soft Tissue (Dental Pack)	Castable Wax; Castable Wax 40
Liqcreate (SLA and DLP)	Stone Coal Black; Deep Blue	Tough-X; Strong-X; Flexible-X; Elastomer-X; Composite-X; Clear Impact	Premium Model; Gingiva Mask; Dental Model Pro Grey; Dental Model Pro Beige	Was Castable
NexDent (LCD)	-	-	NexDent SG; NexDent Ortho IBT; NexDent Ortho Flex; NexDent C&B MFH; NexDent Ortho Rigid; CROENTEC for NextDent; NextDent Ortho Clear; NextDent Model 2.0; NexDent Denture 3D+; NextDent Tray; NextDent Cast; NexDent Try-In; NextDent Gingiva Mask	-
Kudo3D (LCD)	3DSR 405 Black; 3DSR 405 Green; 3DSR 405 Clear; 3DSR 405 White; 3DSR DX resin	3DSR L-405 ENG Tough Grey; 3DSR L-405 Flexible; 3DSR L-405 Engineering Hard; 3DSR Titan Engineering Hard The 3DSR Titan Engineering Tough; 3DSR Titan Flexible resin	3DSR L-405 General Dental	3DSR 405 Castable; 3DSR UHR resin; 3DSR Titan Cast
ResinWorks3D (DLP and LCD)	-	-	-	EasyCast Series 200; EasyCast Series 400
Miicraft BV Resins (DLP)	Model Black; Micro-structure Transparent	IP High-Resistant; Flexible Transparent; Graphy S-100; Graphy Soft 100; Graphy TE-100	Dental Model Caramel	Jewelry Cast UHD GREEN

Resin (Zortrax, Olsztyn, Poland) for UV LCD. The comparison of the base dimensions of the printed MNs revealed that values closer to the intended design geometry (1000 µm) were achieved when using the LCD printer. However, the MNs produced with DLP exhibited an optimal height of 935.8 µm, outperforming the heights of 819.3 µm for SLA and 802 µm for LCD. Furthermore, despite the use of different printing materials, which can indeed influence printing performance, the overall data indicated that the tested DLP printer delivered better resolution compared to SLA and LCD.

VP 3DP technologies are often categorized as heat-free printing techniques primarily because they involve minimal localized heating during the printing process. This characteristic makes them well-suited for incorporating thermo-sensitive and thermo-labile active compounds and drugs into the resin formulations [5,30]. Nonetheless, the application of VP-based 3DP for pharmaceutical drug delivery purposes presents certain challenges, such as the limited availability of photocurable resins suitable for pharmaceutical applications. Additionally, many of these materials are currently not recognized as generally safe (GRAS) for consumption [32]. Among the photocurable polymers that have been most extensively studied for pharmaceutical applications are poly(ethylene glycol) diacrylate (PEGDA), poly(ethylene glycol) dimethacrylate (PEGDMA), poly(2-hydroxyethyl methacrylate), poly(ε-caprolactone) (PCL), and poly(propylene fumarate)/diethyl fumarate (PPF/DEF) [30,32]. However, the main concern when using these polymers is the potential for residual monomers to remain in the final printed products. As a result, it is necessary to conduct residual monomer analysis to ensure the safety and efficacy of pharmaceutical applications involving VP-based 3DP [5].

The toxicity of certain PIs is also a significant concern in VP 3DP. Some of the most extensively studied PIs include those from the Irgacure family (e.g., Irgacure 2959, 2-hydroxy-1-[4-(hydroxyethoxy)phenyl]-2-methyl-1-propanone)), riboflavin, triethanolamine, and diphenyl(2,4,6-trimethylbenzoyl)phosphine oxide (TPO). For example, Williams et al. [33] conducted a study on the cytotoxicity of three UV-sensitive Irgacure PIs (Irgacure 2959, Irgacure 184 (1-hydroxycyclohexyl-1-phenyl ketone), and Irgacure 651 (2,2-dimethoxy-2-phenylacetophenone) across six different cell lines. The results indicated that Irgacure 2959 showed good tolerance in various cell types over a wide range of chemical concentrations.

Riboflavin (vitamin B2) has been explored as a natural alternative to synthetic PIs. It is generally considered non-toxic, highly water-soluble, and capable of absorbing light in the 330–470 nm range, which aligns with the UV range used in SLA printing systems [30]. Nguyen et al. [34] investigated the feasibility of using a PI system comprising riboflavin and

triethanolamine, comparing its efficiency and toxicity with commercially available PIs, Irgacure 369 and Irgacure 2959. The results showed that the novel PI system exhibited higher biocompatibility but lower efficiency in terms of laser fluence.

TPO has also undergone extensive examination as a PI for polymer-based resins. According to research by Kim et al. [35], TPO reduces cell viability in a dose-dependent manner, with high cytotoxicity observed at a concentration of 50 μM. Therefore, it is advisable to exercise caution and avoid higher concentrations of TPO for clinical applications.

In summary, these studies underscore the importance of a careful selection of PIs, considering their potential impact on the biocompatibility and safety of printed products, particularly in the context of pharmaceutical and medical applications [30,33–35].

The application of VP 3DP techniques also holds considerable potential for personalizing pharmaceutical dosage forms, primarily due to their exceptional detail and resolution capabilities. However, a challenge within pharmaceutical applications of VP technologies lies in the inability to simultaneously print with low volumes of different resins. This limitation can lead to time-consuming and cost-inefficient formulation development processes. One current solution to address these challenges involves the adaptation of SLA 3DP devices. For instance, Robles-Martinez et al. [36] introduced an innovative SLA 3DP method to manufacture multi-layer polypills containing six spatially separated drugs (paracetamol, naproxen, caffeine, aspirin, prednisolone and chloramphenicol) with various cylindrical and ring shapes. The authors achieved this by modifying the Form 1+ printer software, incorporating a sequential command input structure, allowing for the inclusion of different resins and drug compositions within the same vehicle structure through a discontinuous printing technique. The OpenFL version of PreForm software was modified to include the following sequential command inputs: (i) resin printing; (ii) pause the printing process upon layer completion; (iii) raise the build platform, enabling resin tray removal; (iv) resin tray replacement for a different resin formulation; (v) lower the build plate to its previous position; and (vi) resume printing to create the next formulation layer. From a different perspective, Curti, et al. [37] developed an SLA apparatus to expedite the screening of pharmaceutical photopolymer resin formulations. They modified a commercially available SLA (Form 2 SLA 3D printer) by designing a novel resin tank and a platform capable of simultaneously printing up to 12 different formulations. This innovation significantly reduced the amount of required sample resin by 20-fold. They also evaluated a pool of 156 placebo formulations to identify printable candidates for use as versatile, multi-purpose, drug-loadable resins, thereby facilitating the creation of safe, effective, and personalized dosage forms. Furthermore, the study assessed resin efficiency recovery, highlighting the critical influence of the platform type and the duration it remains in the 3D printer before removal. Surprisingly, longer platform retention in the printer led to higher recovery efficiency. Additionally, the use of an aluminum-built platform in the novel SLA apparatus reduced the amount of adhering resin by 70.27 % compared to the original one. These findings contribute to optimizing the cost-effectiveness of the process, a vital aspect for the successful integration of 3DP in pharmaceutical settings, particularly considering that the production of personalized dosage forms in clinical environments may entail higher costs compared to mass production at the industrial level.

3.2. *Resins used for topical and transdermal applications*

VP technologies, including SLA, face certain limitations in terms of material options for topical applications. This is because many of the available resins (Table 2) are not officially recognized as safe for such purposes [7]. The most used biocompatible resins are dental and medical device resins, categorized as Class I and Class IIa. These classifications pertain to biocompatibility regulations and refer to the types of materials suitable for various applications. Class I Biocompatible Resins are intended for non-invasive devices that come into contact with intact skin. They are also suitable for appliances meant for transient or short-term use in the oral, ear canal, or nasal cavities. Additionally, Class I resins can be used for reusable surgical instruments. Class IIa Biocompatible Resins are suitable for devices that come into contact with bodily fluids or open wounds. They are also used for devices involved in administering or removing substances from the human body. Moreover, Class IIa biocompatible resins are ideal for short-term invasive devices, such as invasive surgical elements, and for long-term implantable devices that are placed in teeth [38]. The choice of material for products designed for topical application hinges on the specific purpose of the product. If the product will interact with intact skin, Class I resins are appropriate, while open wounds require Class IIa resins.

The development of suitable resins for VP 3DP, particularly for pharmaceutical applications, is indeed an urgent and evolving area. These resins must meet stringent criteria to ensure safety, efficiency, and personalization of vehicles for pharmaceutical applications. According to the Formlabs website, resins for biocompatible applications are developed in alignment with several international standards, including ISO 10993-1:2018, ISO 7405:2009/(R)2015, and ISO 18562-1:2017. Additionally, all biocompatible resins are ISO 13485 and ISO 14971 compliant. Dental and medical device resins, along with the engineering resin Tough 1500, also meet the requirements for biocompatibility with skin for use extending beyond 30 d [39]. This section provides an overview of the most relevant research conducted in the field of topical and transdermal pharmaceutical applications utilizing VP-printed vehicles. It places specific emphasis on the materials employed, encompassing both commercially available resins (Table 3) and lab-made resins (Table 4).

3.2.1. *Commercial resins*

Xenikakis, et al. [40] explored the use of Castable Resin from Formlabs to create SLA-based MNs. The objective was to enhance the transport of solutes with varying molecular weights (Fig. 5A). They focused on two model dyes, Calcein (with a molecular weight of 622.54 Da) and FITC-Dextran (with a molecular weight of 4000 Da). The MNs produced using this specific resin exhibited impressive mechanical properties, such as being able to withstand forces of up to 60 N

Table 3 – Commercial resins.

Photopolymer	3DP Technology	3DP Equipment	Drug/Molecule	Studies	Possible Applications	References
Castable Resin (Formlabs)	SLA	Formlabs1+ (Formlabs, Massachusetts, USA)	Calcein (MW 622.54 Da), FITC-Dextran (MW 4000 Da)	Use of solid castable resin-based 3D MNs printed (SLA), to enhance the transport of solutes with different MW	MNs for transdermal drug delivery	[40]
Class I biocompatible resin, Dental SG (Formlabs)	SLA + IJ	Form 2 (Formlabs, Massachusetts, USA)	Insulin	3D-Printed biocompatible polymeric MNs for transdermal insulin delivery: SLA to print high-quality MNs, IJ to print insulin solutions as fine droplets onto the MNs surface. *Ex vivo* studies.	MNs for transdermal insulin delivery	[41]
Class I biocompatible resin, Dental SG (Formlabs)	SLA + IJ	Form 2 (Formlabs, Massachusetts, USA)	Insulin	Continuation of the work presented in [39]. In vivo studies	MNs for transdermal insulin delivery	[42]
Class I biocompatible resin, Dental SG (Formlabs)	SLA + IJ	Form 2 (Formlabs, Massachusetts, USA)	Insulin	Correlation between design and manufacturing parameters, and MNs quality and drug delivery performance	MNs for transdermal insulin delivery	[43]
Class I biocompatible resin, Dental SG (Formlabs)	SLA	Form 2 (Formlabs, Massachusetts, USA)	Fluorescein (model hydrophilic molecule) Insulin (model drug)	Development of a device (3DMNMEMS) combining 3D printed MNs and MEMS for real-time in situ control of drug administration	3DMNMEMS device for controlled transdermal drug delivery	[44]
Class I biocompatible resin (Formlabs)	SLA + IJ	Form 2 (Formlabs, Massachusetts, USA)	Cisplatin	Manufacture of a polymeric MNs array for cisplatin delivery (skin cancer treatment). SLA used to print the MNs and IJ to coat the MNs surface with cisplatin.	MNs for skin cancer treatment	[45]
Biocompatible class IIa resin, Dental LT Clear (Formlabs)	SLA	Form 2 (Formlabs, Massachusetts, USA)	Rhodamine B, Fluorescein, Methylene Blue (fluorochrome model drug solutions)	Single step fabrication scheme to create hollow MNs interfaced with microfluidic structures using SLA 3D Printing	Microfluidic-enabled hollow MNs device for transdermal delivery	[28]
Biocompatible Class IIa resin, NextDent Ortho Rigid (Nextdent B.V.)	LCD	N.D.	Octreotide acetate (model peptide)	3D-Printing (LCD) of a hollow MN microdevice composed of resin-based array and PLA reservoir for transdermal peptide delivery	MNs for transdermal macromolecular delivery	[46]
3DM-castable resin (Kudo3D Inc.)	DLP	Titan1(Kudo3D Inc., California, USA)	NSAIDs	Development of a dual-function MNs array to act as a splint to immobilize an affected trigger finger and deliver NSAIDs for pain relief	Personalized dual-function MN splint	[47]
MiiCraft BV-007A (Young Optics Inc.)	DLP	MAX X27 DLP (Asiga, Alexandria, Australia)	–	Printing of different solid MN arrays with various geometries and heights using a photocurable microfluidic resin through DLP	Solid MNs	[48]
Clear Resin V4 (Formlabs Inc.,)	SLA	Form 2 (Formlabs, Massachusetts, USA)	–	"Print & Fill" mold fabrication method to obtain high-aspect ratio sharp needles capable of penetrating tissue	Solid MNs for drug delivery	[49]

(*continued on next page*)

Table 3 (*continued*)

Photopolymer	3DP Technology	3DP Equipment	Drug/Molecule	Studies	Possible Applications	References
eShell 200	µSLA	The Perfactory III SXGA+ system (EnvisionTEC GmbH, Gladbeck, Germany) equipped with a Digital Micromirror Device SXGA+ (1280 × 1024-pixel resolution)		Flat conical MNs	Drug delivery for treatment of skin infections	[50]
eShell 200and Gantrez AN-169 BF	µSLA + IJ	Perfactory III SXGA+ (EnvisionTEC GmbH, Gladbeck, Germany)	–	Pyramidal-like MNs built with biodegradable co-polymer	Drug delivery for quantum dots as an antibacterial agent	[51]
eShell 200 and Gantrez AN-169 BF	µSLA + IJ	Perfactory III SXGA+ visible light dynamic mask µSLA system (EnvisionTEC GmbH, Gladbeck, Germany).	–	Continuation of the work presented in [48]	Fabrication of solid biodegradable MNs and a wide range of pharmacologic agent compositions	[52]
eShell 200	TPP	N.D.	Insulin	Conical MNs	Transdermal delivery of insulin	[53]
Photoresist	TPP	Direct laser writing system (Nanoscribe, GmbH, Photo Professonal GT)	–	Magnetic MNs in cylindrical, pyramidal, and conical shapes	MNs coated with iron for applications in tissue engineering, single cell analysis or drug delivery	[54]
IP-S photoresist	TPP	N.D.	–	Hollow MNs	Inside the body implantation, transdermal sampling, or drug delivery applications	[55]
PVP - MNs N.D. - Mold	SLA	Objet Eden350 (Stratasys, Ltd., Edina, MN, USA)	Blue dye	Development of a print-and-shrink technique to create complex shape polymeric MNs	Transdermal delivery	[56]
Sodium alginate or f galactose – MNs MicroChem (SU-8 photoresist) - Mold	SLA	N.D.	*Vitex agnus-castus* and *Tamarindus indica*	Development of dissolvable MNs with encapsulated plant extracts for subcutaneous tissue release, using a SLA/mould fabrication technique	Transdermal approach for anti-cellulite management	[57]
Mg and PVP – MNs PDMS - Mold	SLA	N.D.	IgG antibody (model drug)	Built-in active MNs with enhanced autonomous drug delivery	Transdermal delivery	[58]

LCD, Liquid-crystal display; MW, Molecular weight; N.D, not defined.

while maintaining their structural integrity. Additionally, they displayed elastic behavior, meaning that after the application of force, the original shape of the MNs was restored.

Pere et al. and Economidou et al. have undertaken a series of studies [41–43] focused on the application of Class I biocompatible resin, Dental SG from Formlabs. Their research has focused on creating solid-coated MNs designed for transdermal insulin delivery. This was achieved through a combination of 3DP techniques, specifically IJ for MN array printing and SLA for MN coating. In their most recent study [43], the emphasis was placed on optimizing the 3D-printed MNs. This optimization encompassed two critical aspects: the MN design (with considerations such as geometrical shapes like pyramids, cones, and spears) and the fine-tuning of manufacturing parameters, ranging from printing angles to post-printing curing conditions. The objective was to enhance the quality and performance of the MNs, with a focus on attributes like material strength, sharpness, and drug delivery efficiency. Among the manufacturing parameters, the post-printing curing conditions were identified as influential. They had a direct impact on the mechanical properties of the material and, consequently, the strength of the MNs. This

Table 4 – Lab-made resins.

Photopolymer	*PI*	*PA*	*3DP Technology*	*3DP Equipment*	*Drug/Molecule*	*Studies*	*Possible Applications*	*References*
PEGDA/PEG300	TPO	–	SLA	Form 1 + Stereolithography 3D printer, Formlabs, UK	Salicylic Acid	Evaluate the feasibility of printing size and shape anatomically personalized salicylic acid anti-acne masks using two different printing technologies, FDM and SLA	Anti-acne patches	[59]
PEGDA/PVP	BAPO, ABCV and HHEMP	–	SLA	Pico 2 HD (Asiga)	AHP-3	Potential of DLP 3D printer for fabrication of personalized MNs to deliver a small peptide	Anti-wrinkle small peptide MNs	[60]
PEG	TPO	–	CLIP	S1 CLIP prototype system (Carbon)	Bovine serum albumin, ovalbumin, lysozyme (model proteins)	Spatially controlled coating of MNs for transdermal protein delivery	Protein transdermal delivery	[61]
PEG	TPO	–	CLIP	–	–	Novel technology to rapidly prototype sharp MNs with tunable geometries	Drug delivery	[62]
PEGDA	TPO	–	DLP	Asiga MAX X27 (Asiga Ltd., Alexandria, NSW, Australia)	Sodium diclofenac	Fabrication of intelligent MN arrays	Transdermal delivery	[63]
PEGDA	BPO	Sudan I (Sigma-Aldrich, St. Louis, MO)	Projection µSLA	Custom-built µSLA system	–	MNs with backward-facing barbs to enhance skin adhesivity	Solid MNs for drug delivery	[64]
Ormocer® US-S4	Irgacures® 369	–	TPP	N.D.	–	Development of MN structures for transdermal drug delivery with a larger range of geometries	Hollow MNs	[65]
SR 259 and Ormocer® B59	Irgacures® 369	–	TPP	N.D.	–	Cylindrical MNs with conical tips	Fabrication of antimicrobial MNs using TPP and pulsed laser deposition.	[66]
Ormocer® US-S4	Irgacure® 369	–	TPP	N.D.	–	Development of micromedical devices	MNs as micromedical devices	[67]
SR 610 – MNs SR 259 – Mold	Irgacure® 369	–	TPP	N.D.	Gentamicin sulfate	Combination of TPP and micromolding to fabricate PEG-gentamicin sulfate MNs	MNs with antimicrobial activity	[68]
PEDG400DA	BAPO	–	µSLA	High-precision DLP system from previous work [68]	–	Low-cost, fast method to build hydrogel based MNs	Drug injection	[69]
PPF	DMPA	–	µSLA	Projection-based µSLA system using digital micromirror device (dynamic pattern generator)	–	Fabrication of MNs using multiple materials, including photocurable biodegradable material	Drug delivery	[70]
PPF	BAPO	–	µSLA	Digital micromirror device-based projection system	Dacarbazine	Drug-loaded MN arrays for transdermal delivery of a chemotherapeutic drug	Drug delivery	[71]

DMPA: 2,2-Dimethoxy-2-phenylacetophenone.

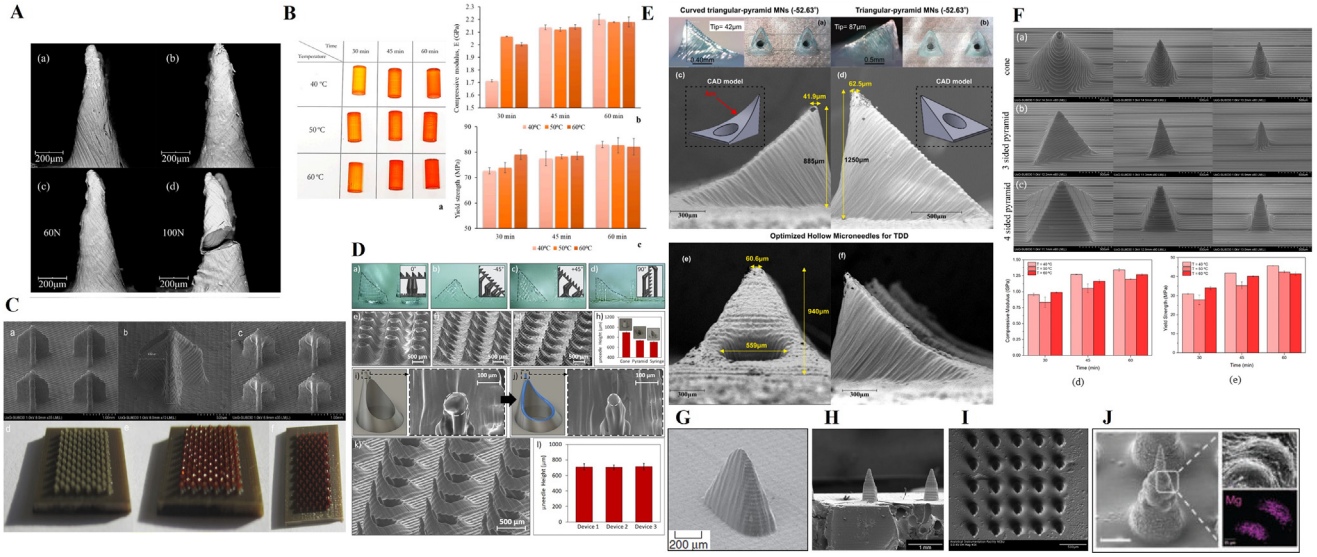

Fig. 5 – Overview of the commercial materials used to create MNs for transdermal applications. (A) Use of solid castable resin-based 3D MNs printed (SLA), to enhance the transport of solutes with different molecular weights. (a and b) MNs before fracture force test. (c and d) MNs after application of 60 N and 100 N axial load, respectively. Reproduced with permission from [40]. (B) Utilization of the Class I biocompatible resin Dental SG (Formlabs) for the development of solid-coated MNs for transdermal insulin delivery using a combination of 3D printing techniques – IJ (MNs array printing) and SLA (MNs coating): Influence of post-printing curing conditions on material's mechanical properties and MNs strength. (a) Digital image of compression specimens for different curing settings, (b) compressive moduli, and (c) yield strengths obtained by specimens subjected to different curing regimes. Reproduced with permission from [43]. (C) Manufacture of a polymeric MNs array (Class I biocompatible resin) for cisplatin delivery (skin cancer treatment). SLA used to print the MNs and IJ to coat the MNs surface with cisplatin. SEM images of uncoated (a and b) and coated (c) 3D printed cross-MNs at various magnifications, where the photopolymerised layers can be clearly seen. Optical images of uncoated (d) and coated with red dye (e and f) 3D printed cross – MN patches. Reproduced with permission from [45]. (D) Single-step fabrication scheme to create hollow MNs using a biocompatible class IIa resin, Dental LT Clear (Formlabs), interfaced with microfluidic structures using SLA 3D Printing. Characterization of 3D-printed hollow MN arrays. Images of sheared-cylinder MNs printed at (a) 0°, (b) −45°, (c) +45°, and (d) 90° angles with outlined profiles (insets show the corresponding print setups). SEM images of the (e) conical, (f) pyramidal, and (g) basic syringe-shaped needle arrays. (h) Average needle heights for each design (for a subset of 25 MNs per array). (i) CAD model of the syringe-shaped design and the SEM image of the tip (~50 wwwμm radius of curvature). (j) CAD model of the fine-tip syringe-shaped design (additional features highlighted) and the SEM image of the tip (~25 μm radius of curvature). (k) SEM image of the fine-tip MN array. (l) Average MN heights across three separate fine-tip MN arrays (for a subset of 25 MNs per array). Error bars indicate ± standard deviation. Reproduced with permission from [28]. (E) 3D-Printing (LCD) of a hollow MN microdevice composed of resin-based array (Biocompatible Class IIa resin, NextDent Ortho Rigid, Nextdent B.V.) and PLA reservoir for transdermal peptide delivery. Optical microscopy and SEM micrographs of optimized curved HMNs (a, c, e, and f) compared with the initial configuration of triangular-pyramid HMNs (b and d). Reproduced with permission from [46]. (F) Printing of different solid MN arrays with various geometries and heights using a photocurable microfluidic resin (MiiCraft BV-007A, Young Optics Inc.) through DLP. SEM images of 3D-printed MNs. (a) Cone, (b) 3-sided pyramid and (c) 4-sided pyramid MNs. Obtained values on (d) compressive modulus and (e) yield strength by exposing all the printed cylinders to different curing settings. Reproduced with permission from [48]. (G) SEM images of eShell 200 MN array structures with 750 mm x 250 mm base and 1000 mm height. Reproduced with permission from [50]. (H) SEM of three unmodified Gantrez R® AN 139 polymer MNs in a five-MN array produced using visible light dynamic mask μSLA-micromolding. Reproduced with permission from [52]. (I) SEM of an eShell 200 MN array created using the TPP microfabrication and following PDMS micromolding process. Reproduced with permission from [53]. (J) SEM image of single active MN tip loaded with Mg particles and energy-dispersive X-ray analysis of the entrapped Mg particles. Scale bars, 300 μm, and 25 μm, respectively. Reproduced with permission from [58].

influence stemmed from the crosslinking degree of the resin (Fig. 5B). Economidou et al. [44] further studied the application of the same biocompatible resin for the development of an innovative, personalized, and highly adaptable device that integrated 3D printed MNs and Microelectromechanical Systems (MEMS). This 3DMNMEMS device enabled real-time, in situ control of drug administration, providing users with a powerful tool for personalized and precise drug delivery.

In another study [45], the combination of 3DP techniques (SLA + IJ) was explored to develop a polymeric MN matrix

designed for cisplatin delivery, as a potential solution for transdermal drug delivery in the context of skin cancer treatment. The chosen polymer for this attempt was also a Class I biocompatible resin. The process involved photopolymerization through SLA, followed by the coating of the MN matrix with cisplatin and the hydrophilic polymer polyvinyl caprolactam–polyvinyl acetate–polyethylene glycol, achieved through IJ printing (Fig. 5C). The study evaluated the printability of the 3D MNs and found that adopting a printing-in-an-angle approach significantly enhanced the reproducibility and overall quality of the final products. Moreover, optical coherence tomography analysis demonstrated the exceptional skin-piercing capability of these MNs, reaching a depth of 80 %.

Yeung et al. [28] introduced a groundbreaking approach for fabricating hollow MNs integrated with microfluidic structures in a single step, employing an SLA-based 3DP technique. They used a biocompatible Class IIa resin, Dental LT Clear from Formlabs, which resulted in MNs characterized by high-printing accuracy and mechanical robustness. To optimize the penetration performance of these MNs, the authors conducted a comprehensive investigation involving several key parameters: (i) Printing Angles: the study explored the impact of different printing angles (0°, −45°, +45° and 90°) while employing a basic sheared-cylinder MN design with a height of 900 µm and a 45° cut, (ii) Different Geometries: the research considered the influence of different MN geometries, including cone, pyramid, and syringe designs; (iii) Radius of Curvature: the authors evaluated the effects of varying the radius of curvature at the needle tip (Fig. 5D).

Xenikakis, et al. [46] conducted a study in which they developed a hollow MN microdevice using LCD-based 3DP. The microdevice was designed to facilitate transdermal macromolecular delivery and was constructed using a biocompatible Class IIa resin, NextDent Ortho Rigid (Nextdent B.V.) array, along with a polylactic acid (PLA) reservoir. Octreotide acetate served as the model peptide for this delivery system. The MNs produced in this study exhibited favorable fracturing characteristics. In their investigation of the most suitable MN geometry for permeation studies, the authors found that the triangular-pyramid design, printed at an angle of 52.63°, was the most promising choice (Fig. 5E). To assess the cytocompatibility of the commercial resin, the researchers conducted tests using human keratinocytes (HaCaT) cells. Some growth inhibition was observed, attributed to certain potentially hazardous components within the resin composition, such as the PI and monomers, which can easily generate free radicals. However, the observed differences between the samples and control groups were not statistically significant. Consequently, the MNs were deemed to be non-cytotoxic, opening the door to their potential use in transdermal drug delivery applications.

In a study by Lim et al. [47], a novel dual-function MN array was introduced, which served as both a splint to immobilize a trigger finger and a drug delivery system for non-steroidal anti-inflammatory drugs (NSAIDs) to provide pain relief. To construct the MNs in this dual-purpose system, the authors employed 3DM-castable resin from Kudo3D Inc. The produced MNs exhibited a high fraction force, equivalent to twice the average force exerted by the thumb. In addition, biocompatibility tests using human dermal cell lines revealed that the MNs were well-tolerated by biological tissues, suggesting their potential for use in clinical applications.

Tabriz et al. [48] used DLP to explore the feasibility of fabricating various solid MN arrays with different geometries and heights, employing the photocurable microfluidic resin known as MiiCraft BV-007A (Young Optics Inc.). The investigation encompassed an assessment of the mechanical properties, piercing capacity, and cytotoxicity of the resin. The DLP printing technology demonstrated exceptional capacity and high resolution for producing MN arrays with diverse geometries, such as cones, three-sided, and four-sided MNs, and varying height-to-base ratios (1:1, 2:1 and 3:1) (Fig. 5Fa- 5Fc). The results also revealed that the mechanical properties of the MNs were influenced by curing temperature and duration. The optimal conditions for achieving the desired mechanical properties were identified at 40 °C for temperature and 60 min for duration (Fig. 5Fd and 5Fe). Additionally, in vitro cytotoxicity studies in human dermal fibroblasts confirmed the excellent biocompatibility of the resin.

Rieger et al. [49] introduced an innovative and customizable approach for manufacturing MN masters to produce female molds, employing a cost-effective 3D SLA printer. The primary goal of this research was to address the limitations often associated with previous MN designs, which typically exhibit low tip radii and low aspect ratios. The authors utilized a UV-curable Clear Resin V4 (Formlabs, Inc.) to fabricate a 3D-printed needle array basin. Subsequently, they poured Grey Resin V4 (Formlabs, Inc.) into the needle array basin to fill it, effectively creating a MN array master. The final step involved pouring silicone over the entire MN array master, leading to the formation of a female mold. This technique, referred to as the "two-step Pint & Fill" mold fabrication method by the authors, resulted in the production of high-aspect ratio needles composed of carboxymethyl cellulose and PLA that possessed sharp tips, making them capable of effectively penetrating tissues. eShell 200 is a Class-IIa biocompatible and water-resistant material, comprising 0.5 %–1.5 % (w/w) of phenylbis (2,4,6-trimethylbenzoyl) phosphine oxide (BAPO) as a PI, 15 %–30 % (w/w) of propylated (2) neopentyl glycoldiacrylate, and 60 %–80 % of urethane dimethacrylate. Gittard et al. [50] and Boehm et al. [51,52] proposed crucial steps for processing eShell 200 MN arrays made of biodegradable acid anhydride co-polymers through µSLA-micromolding. Gittard et al. [50] reported the fabrication of MNs using eShell 200 through µSLA. They emphasized the utility of this 3DP technology for manufacturing MNs that can be coated with antimicrobial agents, namely silver and zinc oxide, for the treatment of localized skin infections (Fig. 5G). Boehm et al. [51,52] employed the same eShell 200 resin to produce master structures using visible light dynamic mask µSLA. They crafted vessels for holding polydimethylsiloxane (PDMS) resin from aluminum crimp top washers to create micromolds. The eShell 200 master structures were affixed to strips of aluminum using cyanoacrylate adhesive. The master arrays were then submerged in the unpolymerized PDMS resin and placed on a 125 °C hotplate for 10 min to initiate polymerization. The production of micromolds was

subsequently completed, and they were filled with an aqueous gel containing the antimicrobial material Gantrez® AN 169 BF (Fig. 5H). This developed MNs system exhibits the potential for treating various skin infections, making it a promising candidate for a wide range of medical applications.

The resin eShell 200 was employed once again by Gittard et al. [53] in a study utilizing TPP technology to create polymer MNs through PDMS micromolding. The process involved creating a negative mold of the MNs array using PDMS, followed by the deposition of approximately 50 µl eShell 200 polymer onto the mold's surface to fabricate the MNs array. This array exhibited adequate compressive strength, making it suitable for use in transdermal drug delivery applications, including transdermal insulin delivery (Fig. 5I). Similarly, the TPP technique was applied in separate studies conducted by Kavaldzhiev et al. [54] and Moussi et al. [55] to manufacture MNs using photoresists, light-sensitive materials composed of a polymer, a sensitizer/inhibitor, and a solvent. In the first study [54], TPP was employed to print cylindrical, pyramidal, and conical needles from a drop-cast IP-Dip photoresist. This process generated high aspect ratio polymer resist MNs on a silicon substrate and allowed for their functionalization with an iron coating, resulting in electromagnetically functional and biocompatible MNs. Moussi et al. [55] proposed the fabrication of various designs of hollow MNs made from IP-S photoresist. The use of TPP and photoresist facilitated the robust and seamless integration of MNs with a chamber or delivery systems.

The research groups of Ochoa [56], Amer [57], and Lopez-Ramirez [58], used SLA 3DP to create molds for the subsequent fabrication of MNs through hydrogel casting and shrinking techniques. Ochoa et al. [56] employed this technique to produce high-resolution polyvinyl pyrrolidone (PVP) biodegradable MNs with intricate geometries suitable for potential vaccine delivery applications. Their MNs demonstrated the ability to penetrate porcine skin to a depth of approximately 100 µm. The Amer group [57] used the SLA-mold fabrication approach to develop dissolvable MNs loaded with plant extracts (*Vitex agnus-castus* and *Tamarindus indica*) for subcutaneous tissue release as part of a transdermal strategy for managing cellulite. They constructed the master mold using MicroChem's SU-8 photoresist resin, while sodium alginate or galactose were investigated as potential MN materials. Sodium alginate showed the most promising preliminary results and was selected for further investigations. Lopez-Ramirez et al. [58] also used SLA 3DP to manufacture built-in active MNs designed for autonomous transdermal drug delivery, with IgG antibody serving as the model drug. In their study, they initially infiltrated magnesium (Mg) microparticles into the negative PDMS mold of the MNs. Subsequently, the model drug and a PVP polymeric matrix were added to create the final product (Fig. 5J).

An overview of commercial resins used in topical and transdermal contexts was provided in Fig. 6. Dental SG (25 %) and eShell 200 (20 %) were identified as the most widely used and versatile in the literature included in this review.

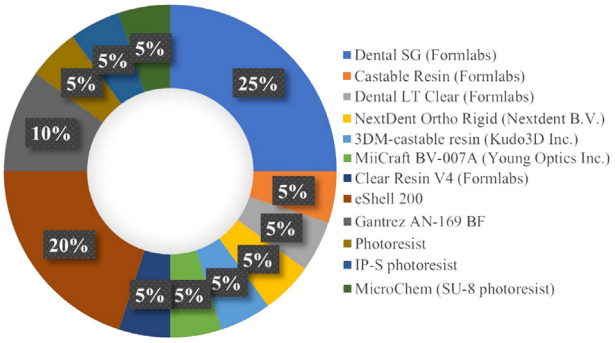

Fig. 6 – Percentages of the commercial resins identified in the articles included in this review.

3.2.2. *Lab-made resins*

Researchers have the option to develop custom resins for VP technology by blending monomers with PIs. The organic phase of these resins primarily comprises dimethacrylates, with commonly used monomers including bisphenol A diglycidyl dimethacrylate, its ethoxylated version, triethylene glycol dimethacrylate, and urethane dimethacrylate. Each monomer exhibits unique polymerization kinetics, and flexural mechanical properties, so selecting the appropriate monomer is crucial in achieving the desired product properties [20]. In addition to monomers, PIs play a vital role in resins, as previously discussed in 1.2. PIs are categorized into two types: type-1 and type-2, differentiated by their radical generation mechanisms; type-1 PIs generate radicals via α-cleavage, while type-2 PIs function through hydrogen abstraction [17,19,20]. Type-1 PIs include TPO and benzoyl peroxide (BPO), while type-2 PIs comprise camphorquinone, phenanthrenequinone, and benzophenone. The PI (PPD, 1-phenyl-1,2 propanedione) combines both radical generation mechanisms. Type-1 PIs absorb high-wavelength UV light, whereas co-initiators and type-2 PIs absorb visible blue light in the range of 400–490 nm. This initiation process is generally slower than that of type-1 PIs and is based on a bimolecular reaction [19]. Similar to monomers, the choice of PI type in the resin significantly influences the final product's properties, including factors such as color stability, 3DP accuracy, degree of conversion, and mechanical properties [35].

The following paragraphs and respective figures present an overview of the type of materials used to create lab-made resins for topical and transdermal applications. Since this is a relatively new technology, publications regarding lab-made resins for topical applications are scarce. The study conducted by Goyanes et al. [59] demonstrated the potential of combining 3D scanning and 3DP for creating personalized anti-acne masks loaded with salicylic acid for topical applications. The authors utilized two different printing technologies, FDM and SLA, to manufacture these masks (Fig. 7A). In the case of SLA, the authors used a photopolymer resin consisting of PEGDA and poly(ethylene glycol) (PEG) as a filler in different ratios (4:6 and 8:2). They incorporated TPO as a PI to facilitate the polymerization process. For FDM the choice was the commercial Flex EcoPLA^{TM} BLUE 45D (flexible PLA) and PCL filaments loaded with salicylic acid. Overall, SLA printing was superior to FDM in terms of resolution, drug loading capacity, thermal stability, and drug diffusion throughout the device. The study highlights the relevance of using SLA technology for

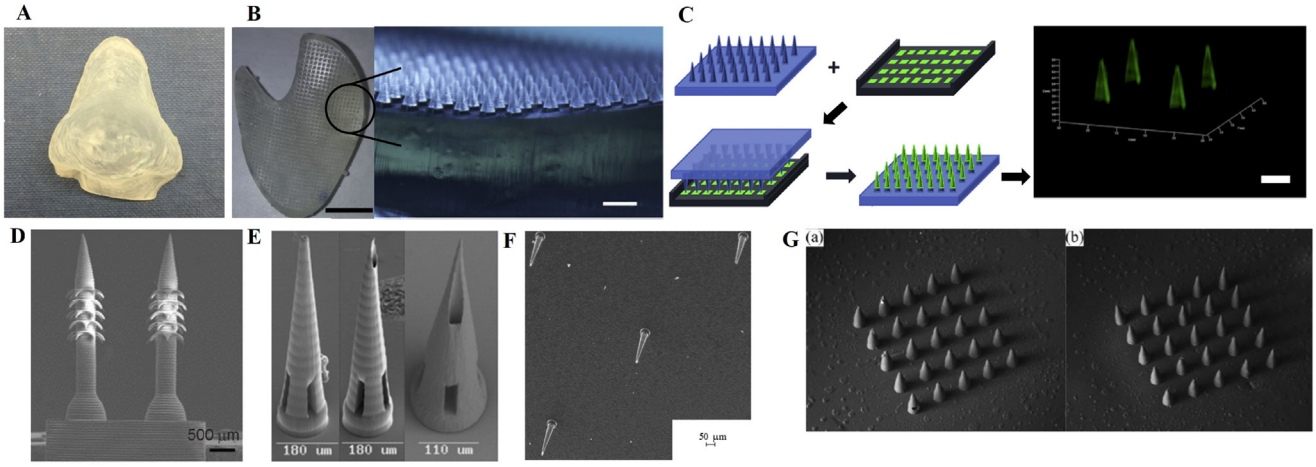

Fig. 7 – Overview of the type of materials used to create lab-made resins for topical and transdermal applications. (A) SLA 3D printed PEGDA/PEG (4:6)-salicylic acid nose-shaped device. Reproduced with permission from [59]. (B) DLP for 3D printing personalized MNs to deliver anti-wrinkle peptide AHP-3 and respective microscope image. Scale bar 1 cm and 1 mm, respectively. Reproduced with permission from [60]. (C) CLIP printed PEG MNs inserted into a solution-filled CMD, then withdrawn and allowed to dry, resulting in coated MNs as shown by the confocal fluorescence image. Scale bar 500 µm. Reproduced with permission from [61]. (D) SEM image of printed MN array with backward-facing barbs. Reproduced with permission from [64]. (E) Scanning electron micrographs of Ormocer® MNs with 0 mm, 1.4 mm and 20.4 mm pore-needle center displacement values (from left to right). Reproduced with permission from. Reproduced with permission from [65]. (F) Scanning electron micrograph of Ormocer® MN array fabricated using TPP. Reproduced with permission from [67]. (G) Scanning electron micrographs of MNs array fabricated with undoped polyethylene glycol 600 diacrylate (a) and MNs array fabricated with gentamicin doped polyethylene glycol 600 diacrylate (b). Scale bar 500 µm. Reproduced with permission from [68].

topical applications, demonstrating that it is not only capable of achieving high resolution but also maintaining flexibility in the printed masks.

For transdermal applications, there is a need to develop high-resolution biocompatible resins with good mechanical strength that have the potential for drug release after loading. The study conducted by Lim et al. [60] addressed this need by exploring the potential of DLP 3DP to create personalized MNs for the delivery of an anti-wrinkle small peptide, acetyl hexapeptide-3 (AHP-3) (Fig. 7B). In this study, the researchers aimed to develop an ideal 3DP material by testing different proportions of PEGDA (MW 700 Da) and PVP. The chosen material was based on factors such as mechanical properties, safety profile of the final polymer, 3DP resolution, rate of drug release, and polymerization rate. The study also assessed three different PIs, including BAPO, Azobis(4-cyanovaleric acid) (ABCV), and 2-Hydroxy-4′-(2-hydroxyethoxy)−2-methylpropiophenone (HHEMP). BAPO was selected as the optimal PI due to its significant absorbance at 405 nm.

The final optimized resin consisted of a 7:3 ratio of PVP:PEGDA and was crosslinked with BAPO. Using this resin, the researchers successfully 3D printed high-quality personalized MNs for an eye patch. These MNs exhibited adequate mechanical strength, reasonable polymerization time, and minimal in vitro cytotoxicity, as assessed in assays with human dermal fibroblast cell lines. The MNs also demonstrated effective skin penetration and remained intact after compression, emphasizing the suitability of the photopolymer system for transdermal applications.

In the study conducted by Caudill et al. [61], CLIP technology was used to develop coated MN patches intended for the transdermal delivery of proteins. The researchers employed three model proteins, namely bovine serum albumin, ovalbumin, and lysozyme, to explore the feasibility of this transdermal delivery approach. To control the spatial deposition and loading of coated protein cargo onto the MNs, the authors developed and employed a coating mask device (CMD) (Fig. 7C). Both the MNs and the CMD were fabricated using a resin composed of PEGDMA with 2.5 wt% of TPO as a PI. The choice of PEGDMA was justified by its insolubility in water and its status as a light-curing derivative of a GRAS material. Overall, the results obtained show that it is possible to control the height of the coating as well as the loading of protein cargo by adjusting the raised edge height of the CMD.

Johnson et al. [62] produced square-shaped pyramidal MNs of varying heights using a model resin composed of trimethylolpropane triacrylate mixed with 2.5 % TPO as a PI. The choice of this resin was based on its composition, as it exhibits fast reactivity and low viscosity properties. The combination of this resin with CLIP technology enabled the rapid fabrication of MNs with diverse sizes, shapes, aspect ratios, spacings, and compositions. This approach was considered the fastest and most versatile MN prototyping method to date.

In the work of Kundu et al. [63], a photopolymer resin was created by mixing PEGDA with TPO as PI. They used DLP technology to 3D print intelligent MN arrays designed for the controlled delivery of sodium diclofenac. The study included optimization of the printing conditions, focusing

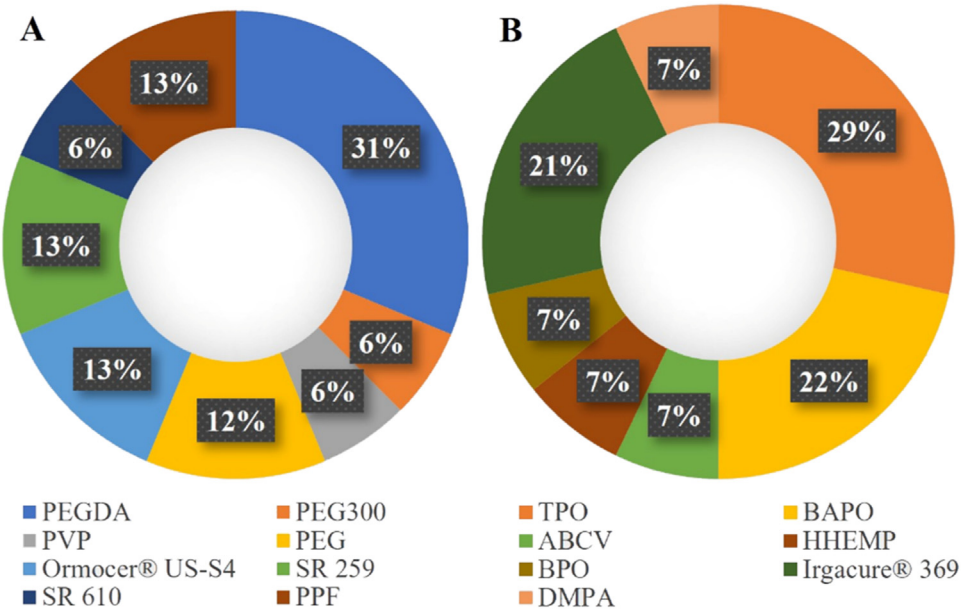

Fig. 8 – Percentages of photopolymers (A) and PIs (B) identified in the articles included in this review.

on achieving an array with high mechanical strength while retaining hydrogel properties that could respond to external physical stimuli such as changes in temperature and pH. Each type of stimulus triggered distinct release characteristics from the MNs, enabling controlled drug delivery. *Ex vivo* experiments using dermatomed human skin showed the MN array's effectiveness in penetrating the skin by disrupting the stratum corneum, thus facilitating transdermal drug delivery.

Han et al. [64] employed μSLA technology to create MNs featuring bioinspired backward-facing curved barbs to enhance tissue adhesion (Fig. 7D). The resin developed for this purpose consisted of biocompatible components. It included PEGDA as a monomer, BPO as a PI, and Sudan I as a photoabsorber (PA). This resin was then used for the 3D printing of the specialized MNs. The study's results showed that the tissue adhesion of the backward-facing barbed MNs was 18 times stronger than barbless MNs. Additionally, it was found that these MNs facilitated sustained drug release within the tissue, which holds significant promise for drug delivery applications. Several studies have reported the use of modified ceramics, specifically Ormocer® resins, to create MN arrays using TPP printing technology. The application of these unique resins, combined with PIs, has shown promise for manufacturing MNs with various sizes and shapes [65–67]. Ovsianikov et al. [65] and Doraiswamy et al. [67] both employed Ormocer® US-S4 resin in combination with Irgacure® 369 as the PI to produce MN arrays (Fig. 7E and 7F, respectively). Their work demonstrated the utility of TPP for creating medical microdevices with a wide range of sizes and shapes. Gittard et al. [66] used Ormocer® b59 for the MN master and Ormocer® SR 259 (PEGDMA) for the MN array. They also incorporated Irgacure® 369 as the PI. This study highlighted the versatility of TPP in generating MNs with varied geometries and sizes. A subsequent study by Gittard et al. [68] described the production of MN mold and array using TPP. They employed SR 259 mixed with 2 wt% Irgacure 369 as the PI for the MN mold and SR 610 (PEG600DA) with the same PI concentration, along with aqueous gentamicin sulfate, for the MN array. This approach resulted in uniform MN arrays suitable for transdermal delivery with added antimicrobial properties to reduce the risk of skin infections (Fig. 7G).

In a more recent study [69], researchers developed hydrogel MNs using high-precision DLP 3DP. The resin was prepared by mixing polyethylene glycol diacrylate (PEG400DA monomer) with 1 wt% BAPO) as the PI. The aim was to create biocompatible MNs capable of both drug injection and retention. This study presented a cost-effective and rapid method for fabricating MNs with favorable mechanical properties, highlighting their potential for clinical applications.

Finally, Yun et al. [70] and Lu et al. [71] utilized the same technology and polymer, μSLA and propylene fumarate (PPF), respectively, to fabricate MNs for different purposes. Yun's paper outlines the framework of μSLA apparatus capable of fabricating MNs using multiple materials, including integrating a photocurable biodegradable material like PPF. The authors also introduce crucial process parameters for achieving precise micro-needle fabrication. The study concludes by validating the system's efficacy, presenting examples of MNs fabricated with PPF. Lu et al., engineered drug-loaded MNs arrays designed for transdermal administration of a chemotherapeutic agent. The arrays featured twenty-five precision-oriented PPF MNs on a single polymeric substrate where Dacarbazine, a commonly employed treatment for skin cancer, was uniformly integrated into the PPF solution before cross-linking. Each MN exhibited a cylindrical base measuring 700 μm in height and a conical tip with a height of 300 μm. This research contributes

valuable insights into developing biodegradable MNs through advanced manufacturing techniques, with potential applications in transdermal delivery.

Similarly to the previous section, we identified in the literature the most used photopolymer - PEGDA (31 %), and PIs - TPO (29 %), BAPO (22 %) and Irgacure 369 (21 %) (Fig. 8).

4. Conclusions and final remarks

In this review article, a wide range of VP-based 3DP techniques were explored, with a particular focus on their potential for developing topical and transdermal products. The primary emphasis was on the materials used in these technologies. Most of the studies examined in this review concentrated on the fabrication of transdermal devices employing MN arrays, indicating the strong interest and potential of MN-based drug delivery systems. Furthermore, many researchers have been using commercially available resins for their 3DP applications, due to convenience but also due to the current limited availability of specialized resins for topical and transdermal use. However, there is an emerging trend of custom resin development, with some authors already exploring the development of custom resins to overcome possible biocompatibility and printing accuracy issues. As 3DP technologies continue to gain popularity for personalization and customization, it is expected that manufacturers will invest in modified printing apparatus that can simultaneously handle different resins and compound types. This would reduce formulation development time and costs. VP-based 3DP technologies offer several advantages, such as low printer and material costs, rapid fabrication, high surface quality, accuracy, and fine resolution. Additionally, they can be used to create vehicles that incorporate thermo-sensitive and thermo-labile compounds. VP-based 3DP technologies hold great promise for the development of topical and transdermal products. While some challenges exist, such as limited resin availability and biocompatibility concerns, the advantages they offer make them an attractive option for various pharmaceutical applications. As the field advances, it is likely that more specialized resins will become available, further expanding the capabilities of these technologies in pharmaceutical research and development.

Overall, significant advancements are anticipated in the development of new VP-based principle techniques. However, it is equally fundamental to invest in the research and development of biocompatible and high-performance resin-based materials for topical and transdermal applications. This involves, for example, establishing guidelines for the selection of resin components, a critical aspect that can significantly impact safety and efficacy. Furthermore, the expectations extend to progress in the regulation of these techniques, encompassing a diverse range of 3D printing technologies.

Conflicts of interest

All the authors declare no conflict of interest.

Acknowledgments

This research was funded by the Fundação para a Ciência e Tecnologia, Portugal [UIDB/04138/2020 and UIDP/04138/2020 to iMed.ULisboa, CEECINST/00145/2018 to J Marto, fellowship 2020.10138.BD to A. Graça and UI/BD/153624/2022 to S. Bom].

REFERENCES

[1] Bom S, Martins AM, Ribeiro HM, Marto J. Diving into 3D (bio)printing: a revolutionary tool to customize the production of drug and cell-based systems for skin delivery. Int J Pharm 2021;605:1–20.
[2] Bom S, Ribeiro R, Ribeiro HM, Santos C, Marto J. On the progress of hydrogel-based 3D printing: correlating rheological properties with printing behaviour. Int J Pharm 2022;615:1–14.
[3] Xu X, Awad A, Robles-Martinez P, Gaisford S, Goyanes A, Basit AW. Vat photopolymerization 3D printing for advanced drug delivery and medical device applications. J Control Release 2021;329:743–57.
[4] Kafle A, Luis E, Silwal R, Pan HM, Shrestha PL, Bastola AK. 3D/4D printing of polymers: fused deposition modelling (FDM), selective laser sintering (SLS), and stereolithography (SLA). Polymers 2021;13:1–37.
[5] Vithani K, Goyanes A, Jannin V, Basit AW, Gaisford S, Boyd BJ. An overview of 3D printing technologies for soft materials and potential opportunities for lipid-based drug delivery systems. Pharm Res 2019;36:1–50.
[6] Arifin N, Sudin I, Ngadiman NHA, Ishak MSA. A Comprehensive review of biopolymer fabrication in additive manufacturing processing for 3D-tissue-engineering scaffolds. Polymers 2022;14:1–22.
[7] Pagac M, Hajnys J, Ma QP, Jancar L, Jansa J, Stefek P, et al. A review of vat photopolymerization technology: materials, applications, challenges, and future trends of 3D printing. Polymers 2021;13:1–20.
[8] Skoog SA, Goering PL, Narayan RJ. Stereolithography in tissue engineering. J Mater Sci Mater Med 2014;25:845–56.
[9] Shen Y, Tang H, Huang X, Hang R, Zhang X, Wang Y, et al. DLP Printing photocurable chitosan to build bio-constructs for tissue engineering. Carbohydr Polym 2020;235:1–9.
[10] Lemma ED, Spagnolo B, De Vittorio M, Pisanello F. Studying cell mechanobiology in 3D: the two-photon lithography approach. Trends Biotechnol 2019;37:358–72.
[11] 3D printing technologies: comparing SLA vs. DLP vs. PμSL. BMF 2022; Availiable from: https://bmf3d.com/resource/comparing-3d-printing-technology
[12] Detamornrat U, McAlister E, Hutton ARJ, Larrañeta E, Donnelly RF. The role of 3D printing technology in microengineering of microneedles. Small 2022;18:1–29.
[13] Kim SY, Shin YS, Jung HD, Hwang CJ, Baik HS, Cha JY. Precision and trueness of dental models manufactured with different 3-dimensional printing techniques. Am J Orthod Dentofac Orthop 2018;153:144–53.
[14] Kelly B, Bhattacharya I, Heidari H, Hossein Shusteff M, Spadaccini C, et al. Volumetric additive manufacturing via tomographic reconstruction. Science 2019;363:1075–9.
[15] Regehly M, Garmshausen Y, Reuter M, König NF, Israel E, Kelly DP, et al. Xolography for linear volumetric 3D printing. Nature 2020;588:620–4.
[16] Weng Z, Huang X, Peng S, Zheng L, Wu L. 3D printing of ultra-high viscosity resin by a linear scan-based vat photopolymerization system. Nat Commun 2023;14:1–9.

[17] Ribas-Massonis A, Cicujano M, Duran J, Besalú E, Poater A. Free-radical photopolymerization for curing products for refinish coatings market. Polymers 2022;14:1–20.
[18] Mondschein RJ, Kanitkar A, William CB, Verbridge SS, Long TE. Polymer structure-property requirements for stereolithographic 3D printing of soft tissue engineering scaffolds. Biomater 2017;140:170–88.
[19] Kowalska A, Sokolowski J, Bociong K. The photoinitiators used in resin based dental composite—a review and future perspectives. Polymers 2021;13:1–17.
[20] Gajewski VES, Pfeifer CS, Fróes-Salgado NRG, Boaro LCC, Braga RR. Monomers used in resin composites: degree of conversion, mechanical properties and water sorption/solubility. Braz Dent J 2012;23:508–14.
[21] Kim D, Shim J, Lee D, Shin S, Nam N. Effects of post-curing time on the mechanical and color properties of three-dimensional printed crown and bridge materials. Polymers 2020;12:1–20.
[22] 3DEXPERIENCE MAKE. SLA 3D printing materials compared. Availiable from: https://www.3ds.com/make/solutions/blog/sla-3d-printing-materials-compared.
[23] Formlabs. Formlabs stereolithography 3D printers. Availiable from 2024: https://impacsystems.com/wp-content/uploads/2024/06/ISE_Form-Printers-Data-Sheet.pdf.
[24] Kudo3D. Resin Archives. Availiable from 2024: https://www.kudo3d.com/product-category/resin/.
[25] Next Dent by 3D Systems. 3D printing materials. Availiable from: https://nextdent.com/.
[26] Miicraft. Products. 2024 Availiable from: https://miicraft.ca/products/resins/.
[27] Yeung C, Chen S, King B, Lin H, King K, Akhtar F, et al. A 3D-printed microfluidic-enabled hollow microneedle architecture for transdermal drug delivery. Biomicrofluidics 2019;13:1–11.
[28] Melchels FPW, Feijen J, Grijpma DW. A review on stereolithography and its applications in biomedical engineering. Biomater 2010;31:6121–630.
[29] Karakurt I, Aydoğdu A, Çıkrıkcı S, Orozco J, Lin L. Stereolithography (SLA) 3D printing of ascorbic acid loaded hydrogels: a controlled release study. Int J Pharm 2020;584:1–9.
[30] Mathew E, Pitzanti G, Gomes dos Santos AL, Lamprou DA. Optimization of printing parameters for digital light processing 3D printing of hollow microneedle arrays. Pharmaceutics 2021;13:1–14.
[31] Wang J, Goyanes A, Gaisford S, Basit AW. Stereolithographic (SLA) 3D printing of oral modified-release dosage forms. Int J Pharm 2016;503:207–12.
[32] Williams CG, Malik AN, Kim TK, Manson PN, Elisseeff JH. Variable cytocompatibility of six cell lines with photoinitiators used for polymerizing hydrogels and cell encapsulation. Biomater 2005;26:1211–18.
[33] Nguyen AK, Gittard SD, Koroleva A, Schlie S, Gaidukeviciute A, Chichkov BN, et al. Two-photon polymerization of polyethylene glycol diacrylate scaffolds with riboflavin and triethanolamine used as a water-soluble photoinitiator. Regen Med 2013;8:725–38.
[34] Kim GT, Go HB, Yu JH, Yang SY, Kim KM, Choi SH, et al. Cytotoxicity, colour stability and dimensional accuracy of 3D printing resin with three different photoinitiators. Polymers 2022;14:1–16.
[35] Robles-Martinez P, Xu X, Trenfield SJ, Awad A, Goyanes A, Telford R, et al. 3D printing of a multi-layered polypill containing six drugs using a novel stereolithographic method. Pharmaceutics 2019;11:1–16.
[36] Curti C, Kirby DJ, Russell CA. Stereolithography apparatus evolution: enhancing throughput and efficiency of pharmaceutical formulation development. Pharmaceutics 2021;13:1–16.
[37] Protolabs Net work by Hub. What's the right resin for SLA? 3D printing materials compared. Availiable from: 2024 https://www.hubs.com/knowledge-base/sla-3d-printing-materials-compared/.
[38] Formlabs. Certifications and standards. Availiable from: 2024 https://support.formlabs.com/s/article/Certifications-and-standards?language=en_US#medical-device.
[39] Xenikakis I, Tzimtzimis M, Tsongas K, Andreadis D, Demiri E, Tzetzis D, et al. Fabrication and finite element analysis of stereolithographic 3D printed microneedles for transdermal delivery of model dyes across human skin in vitro. Eur J Pharm Sci 2019;137:1–11.
[40] Pere CPP, Economidou SN, Lall G, Ziraud C, Boateng JS, Alexander BD, et al. 3D Printed microneedles for insulin skin delivery. Int J Pharm 2018;544:425–32.
[41] Economidou SN, Pere CPP, Reid A, Uddin MJ, Windmill JFC, Lamprou DA, et al. 3D printed microneedle patches using stereolithography (SLA) for intradermal insulin delivery. Mater Sci Eng C Mater Biol Appl 2019;102:743–55.
[42] Economidou SN, Pere CPP, Okereke M, Douroumis D. Optimisation of design and manufacturing parameters of 3D printed solid microneedles for improved strength, sharpness, and drug delivery. Micromachines 2021;12:1–16.
[43] Economidou SN, Uddin J, Marques MJ, Douroumis D, Ting W, Li H, et al. A novel 3D printed hollow microneedle microelectromechanical system for controlled, personalized transdermal drug delivery. Addit Manuf 2021;38:1–11.
[44] Uddin MJ, Scoutaris N, Economidou SN, Giraud C, Chowdhry BZ, Donnelly RF, et al. 3D printed microneedles for anticancer therapy of skin tumours. Mater Sci Eng C 2020;107:1–12.
[45] Xenikakis I, Tsongas K, Tzimtzimis EK, Zacharis K, Theodoroula N, Kalogianni EP, et al. Fabrication of hollow microneedles using liquid crystal display (LCD) vat polymerization 3D printing technology for transdermal macromolecular delivery. Int J Pharm 2021;597:1–14.
[46] Lim SH, Ng JY, Kang L. Three-dimensional printing of a microneedle array on personalized curved surfaces for dual-pronged treatment of trigger finger. Biofabrication 2017;9:1–14.
[47] Tabriz AG, Viegas B, Okereke M, Uddin MJ, Lopez EA, Zand N, et al. Evaluation of 3D printability and biocompatibility of microfluidic resin for fabrication of solid microneedles. Micromachines 2022;13:1–16.
[48] Krieger KJ, Bertollo N, Dangol M, Sheridan JT, Lowery MM, O'Cearbhaill ED. Simple and customizable method for fabrication of high-aspect ratio microneedle molds using low-cost 3D printing. Microsystems Nanoeng 2019;42:1–14.
[49] Gittard SD, Miller PR, Jin C, Martin TN, Boehm RD, Chisholm BJ, et al. Deposition of antimicrobial coatings on microstereolithography-fabricated microneedles. JOM 2011;63:59–68.
[50] Boehm RD, Miller PR, Singh R, Shah A, Stafslien S, Daniels J, et al. Indirect rapid prototyping of antibacterial acid anhydride copolymer microneedles. Biofabrication 2012;4:1–10.
[51] Boehm RD, Miller PR, Hayes SL, Monteiro-Riviere NA, Narayan RJ. Modification of microneedles using inkjet printing. AIP Adv 2011;1:1–10.
[52] Gittard SD, Ovsianikov A, Monteiro-Riviere NA, Lusk J, Morel P, Minghetti P, et al. Fabrication of polymer microneedles using a two-photon polymerization and micromolding process. J Diabetes Sci Technol 2009;3:304–11.
[53] Kavaldzhiev M, Perez JE, Ivanov Y, Bertoncini A, Liberale C, Kosel J. Biocompatible 3D printed magnetic micro needles. Biomed Phys Eng Express 2017;3:1–10.

[54] Moussi K, Bukhamsin A, Hidalgo T, Kosel J. Biocompatible 3D printed microneedles for transdermal, intradermal, and percutaneous applications. Adv Eng Mater 2020;22:1–10.
[55] Ochoa M, Zhou J, Rahimi R, Badwaik V, Thompson D, Ziaie B. Rapid 3D-print-and-shrink fabrication of biodegradable microneedles with complex geometries. In: 2015 Transducers -2015 18th International Conference on Solid-State Sensors, Actuators and Microsystems; 2015. p. 1252–4.
[56] Amer RI, El-Osaily GH, Bakr RO, El Dine RS, Fayez AM. Characterization and pharmacological evaluation of anti-cellulite herbal product(s) encapsulated in 3d-fabricated polymeric microneedles. Sci Rep 2020;10:1–16.
[57] Lopez-Ramirez MA, Soto F, Wang C, Rueda R, Shukla S, Silva-Lopez C, et al. Built-in active microneedle patch with enhanced autonomous drug delivery. Adv Mater 2020;32:1–10.
[58] Goyanes A, Det-Amornrat U, Wang J, Basit AW, Gaisford S. 3D scanning and 3D printing as innovative technologies for fabricating personalized topical drug delivery systems. J Control Release 2016;234:41–8.
[59] Lim SH, Kathuria H, Amir MHB, Zhang X, Duong HTT, Ho PCL, et al. High resolution photopolymer for 3D printing of personalised microneedle for transdermal delivery of anti-wrinkle small peptide. J Control Release 2020;329:907–18.
[60] Caudill CL, Perry JL, Tian S, Luft JC, DeSimone JM. Spatially controlled coating of continuous liquid Interface production microneedles for transdermal protein delivery. J Control Release 2018;284:122–32.
[61] Johnson AR, Caudill CL, Tumbleston JR, Bloomquist CJ, Moga KA, Ermoshkin A, et al. Single-step fabrication of computationally designed microneedles by continuous liquid interface production. PLoS One 2016;11:1–17.
[62] Kundu A, Arnett P, Bagde A, Azim N, Kouagou E, Singh M, et al. DLP 3D Printed “intelligent” microneedle array (iμNA) for stimuli responsive release of drugs and its in vitro and *ex vivo* characterization. J Microelectromechanical Syst 2020;29:685–91.
[63] Han D, Morde RS, Mariani S, La Mattina AA, Vignali E, Yang C, et al. 4D Printing of a bioinspired microneedle array with backward-facing barbs for enhanced tissue adhesion. Adv Funct Mater 2020;30:1–12.
[64] Ovsianikov A, Chichkov B, Mente P, Monteiro-Riviere NA, Doraiswamy A, Narayan RJ. Two photon polymerization of polymer-ceramic hybrid materials for transdermal drug delivery. Int J Appl Ceram Technol 2007;4:22–9.
[65] Gittard SD, Narayan RJ, Jin C, Ovsianikov Q, Chichkov BN, Monteiro-Riviere NA, et al. Pulsed laser deposition of antimicrobial silver coating on Ormocer microneedles. Biofabrication 2009;1:1–6.
[66] Doraiswamy A, Jin C, Narayan RJ, Mageswaran P, Mente P, Modi R, et al. Two photon induced polymerization of organic-inorganic hybrid biomaterials for microstructured medical devices. Acta Biomater 2006;2:267–75.
[67] Gittard S, Ovsianikov A, Akar H, Chichkov B, Monteiro-Riviere NA, Stafslien S, et al. Two photon polymerization-micromolding of polyethylene glycol-gentamicin sulfate microneedles. Adv Eng Mater 2010;12:1–6.
[68] Yao W, Li D, Zhao Y, Zhan Z, Jin G, Liang H, et al. 3D Printed multi-functional hydrogel microneedles based on high-precision digital light processing. Micromachines 2020;11:1–11.
[69] Yun H, Kim H. Development of DMD-based micro-stereolithography apparatus for biodegradable multi-material micro-needle fabrication. J Mech Sci Technol 2013;27:2973 –8.
[70] Lu Y, Mantha SN, Crowder DC, Chinchilla S, Shah KN, Yun YH, et al. Microstereolithography and characterization of poly(propylene fumarate)-based drug-loaded microneedle arrays. Biofabrication 2015;7:1–14.